The Institution of Engineering and Technology

Article

Efficient Hysteresis Characterization and Prediction in 3D-Printed Magnetic Materials Using Deep Learning

Michele Lo Giudice [1,*], Alessandro Salvini [1], Marco Stella [4], Fausto Sargeni [2], Silvia Licciardi [3], Guido Ala [3], Pietro Romano [3], Vittorio Bertolini [4] and Antonio Faba [4]

[1] Department of Civil, Computer Science and Aeronautical Technologies Engineering, Roma Tre University, Roma, 00146, Italy
[2] Department of Electronic Engineering, University of Rome Tor Vergata, Roma, 00133, Italy
[3] Department of Engineering, University of Palermo, Palermo, 90100, Italy
[4] Department of Engineering, University of Perugia, Perugia, 06125, Italy
* Correspondence: michele.logiudice@uniroma3.it;

Abstract: This research proposes a data processing pipeline employing Fourier analysis and deep neural networks to replicate the phenomenon of magnetic hysteresis in particular frequency components derived from experimental data gathered using a newly developed 3D-printed material. The characterization of hysteresis is essential for enhancing material performance and constructing precise models to anticipate material behaviour under diverse operating circumstances, especially in 3D-printed materials where properties can be meticulously regulated to ensure successful applications. The experimental signals were used for training and testing a neural network, exploiting Fourier coefficients to condense signals into the frequency components. This compression extracts fewer parameters and thus reduces and optimises the resources required by the neural network. It also improves the generalisation performance of the model, allowing it to make more accurate predictions on unseen data. This therefore optimises traditional modelling that requires a complete representation of hysteresis loops in the time domain, which must be addressed with the use of complex neural networks and large datasets. The experimental results show lower computational costs during the prediction process and a smaller memory footprint. Furthermore, the proposed model is easily adaptable for the loss estimation in different types of materials and input signals.

Keywords: Magnetic hysteresis; Neural Network; Fourier Transform; Additive Manufacturing

Citation: Lastname, F.; Lastname, F.; Lastname, F. Efficient Hysteresis Characterization and Prediction in 3D-Printed Magnetic Materials Using Deep Learning. *Journal Not Specified* **2024**, *1*, 0. https://doi.org/

Received:
Revised:
Accepted:
Published:

1. Introduction

The building processes of the soft magnetic components for energy conversion systems are under investigation thanks to the new opportunities introduced by the Additive Manufacturing (AM). This young and interesting technology presents some advantages in comparison with the traditional ones, which are, new and higher-performing alloys, waste material reduction, material recycling, and geometries that can be created with greater complexity. The intense and diffused studies performed in the last years by many researchers have produced some encouraging results from the industry point of view. For instance, in the alloys for electrical machines and electrical actuators, new FeSi magnetic cores with an increased percentage of silicon have been experimented with significant power loss reduction in the energy conversions [1–4]. Moreover, some prototypes have been realized by means of AM and experimentally characterized to give interesting information about the potentialities and usability. Magnetic cores have been realized experimentally for transformers, induction motors, reluctance motors and axial flux motors [5–8]. The potentialities of these kinds of material have not been fully investigated and understood, so they are still object of several research activities. In particular, to further improve this promising technology, accurate and effective numerical tools could be useful to simulate and predict the magnetic behaviour of the components before the printing process. Until now the most used and widespread approaches are the Preisach model [9], the Jiles-Atherton model [10], the Play model [11] and some others [12]. All these models are phenomenological-based, they are inspired by the hysteresis phenomena of the magnetic materials, and they try to reconstruct the magnetization processes simulating the physics of the magnetism. In recent years, a different approach with a change of paradigm is under investigation, that is the use of Artificial Intelligence (AI). In particular, Artificial Neural Networks (ANNs) are very promising [13–15]. Their architecture and implementation can be completely independent from the physical behaviour of the material under investigation, which is often very complex, intricate and difficult to represent. In this sense, neural networks represent a mathematical tool which purpose is to optimize the relationships between generic inputs and outputs, independently by the nature (physical or not) of the inputs themselves. The ANNs training can be performed using a suitable experimental data set of a specific magnetic component, after that, they can simulate its magnetic behaviour taking into account different patterns of excitations.

In this work, we propose an ANN and Fourier analysis combination. This approach can reduce the complexity order of the computational tasks, increasing the precision and effectiveness of the results. This methodology is limited to the prediction of the magnetic processes of a specific component with material composition, shape and dimensions defined a priori. On the other hand, it can generalize the magnetic behaviour of the components to many different operational modes.

2. Materials and Experimental Measurements

The magnetic component under investigation in this paper is a FeSi toroidal core. This component has been made by means of Laser Powder Bed Fusion (L-PBF). The specific element involved in addition to iron, and the corresponding percentage in weight are Si 3.7%, Mn 0.3%, Cr 0.16%, Ni 0.02%, and C 0.01%. Through this technique, the magnetic component is made layer by layer using a specific printing device. The powder of FeSi alloy, which consists of nearly spherical particles with a median diameter of 38 μm, is spread on a flat surface and a suitable laser beam melts the magnetic particles for a specific area. A new layer of powder is spread over the subsequent melting process, and so on until the complete realization of the toroid. The laser power was 350 W, while the scanning velocity was 750 mm/s. The thermal treatment was performed in a graphite chamber vacuum furnace to improve the magnetic properties of the sample after the printing procedure. The annealing temperature was 1200 °C for 60 minutes and the heating rate was 5 °C/min. The toroidal sample obtained as described above is shown in Fig. 1. The inner diameter is 50 mm, the outer diameter is 60 mm and a square section of side 5 mm.

Figure 1. FeSi toroidal sample made by additive manufacturing using the L-BPF technique.

The magnetic characterization of this component is necessary for the ANN training and subsequent assessment. We used the volt-ampere method that allows the magnetic field and magnetic induction measurement for the material under investigation. In the Fig. 2 the measurement scheme is represented.

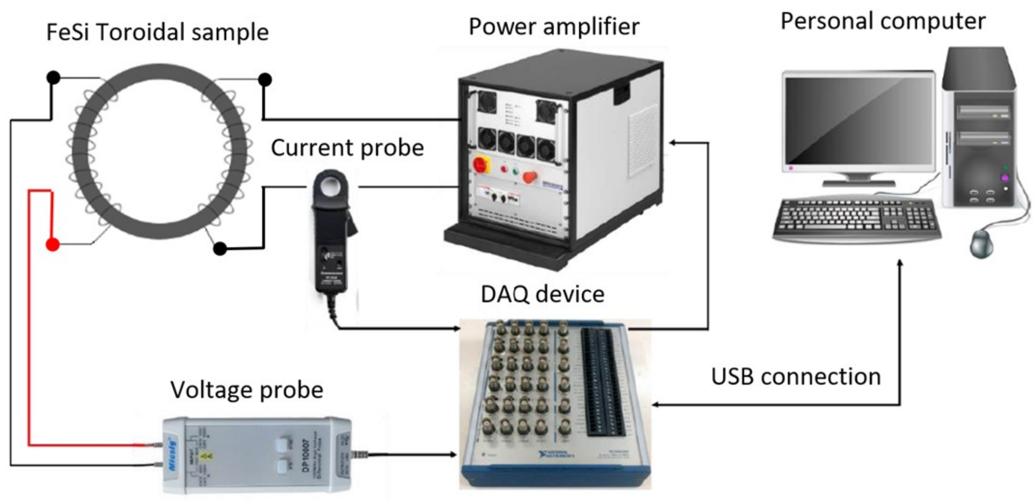

Figure 2. Experimental set-up for the magnetic characterization of the toroidal sample made by additive manufacturing.

Two coils are wounded on the toroidal core, therefore the material is magnetically excited with a superimposed current using the first one, while the corresponding induced voltage is measured on the second one. The magnetic field and the magnetic induction are computed using the equations (1) and (2)

$$H(t) = \frac{Ni(t)}{l} \tag{1}$$

$$B(t) = \frac{1}{NS} \int v(t)dt \tag{2}$$

where *H(t)* is the magnetic field versus time, *B(t)* is the magnetic induction versus time, *N* is the number of turns of both primary and secondary winding, *S* is the area of the sample cross-section, and *l* is the mean length of the sample. Moreover, a digital feedback control has been implemented to make sinusoidal the magnetic induction waveform as indicated in the reference standard [16]. A dataset consisting of 17 hysteresis cycles was generated through a series of magnetic characterisation measurements. The experimental setup adopted provided the simultaneous acquisition of *B(t)* and *H(t)* signals at a sampling rate of 501 Hz. The resulting dataset, which was used for training the neural network, is organised in a matrix of 501 rows and 2 columns, corresponding to the time evolution of the magnetic induction and magnetic field signals, respectively. Fig. 3 offers a comprehensive representation of the dataset, highlighting the sinusoidal waveform of the magnetic induction at 1 Hz in the centre. At the two sides, the output signal and a combined representation of the both signals are displayed respectively, allowing the hysteresis cycles in the *B(t)*-*H(t)* plane to be clearly appreciated. The choice of such a low frequency allows the static hysteresis of the material to be analysed, minimising the influence of parasitic phenomena.

2.1. Fourier analysis and decomposition

Fourier analysis provides a foundational approach for decomposing a signal into its fundamental sinusoidal components. Each component, characterized by distinct frequencies, can be analysed individually and then combined to recreate the original signal. In addition, the selective removal of frequency components effectively reduces noise in the reconstructed signal [17]. A periodic function $f(x)$ with period p can be expressed as a Fourier series:

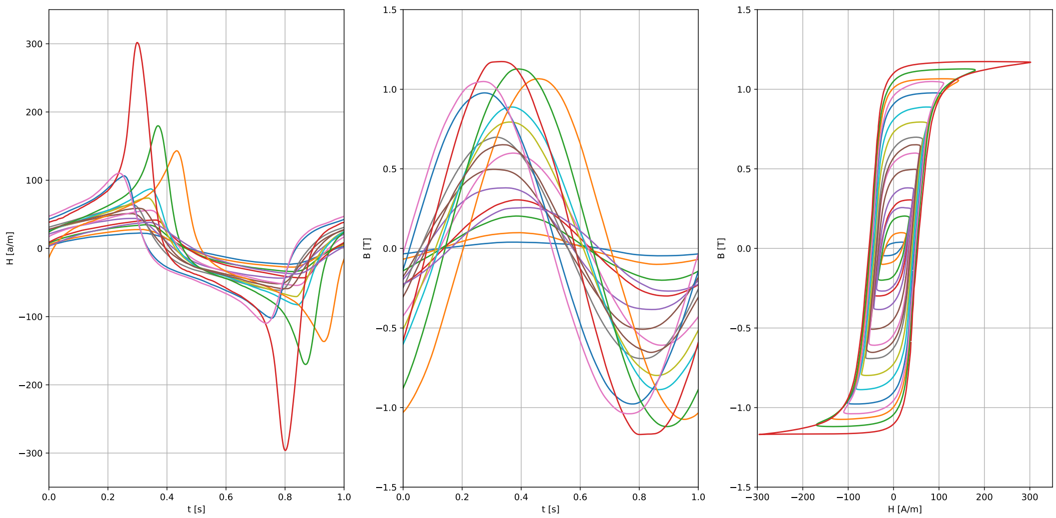

Figure 3. Magnetic field, magnetic induction and the corresponding hysteresis loops measured for the toroidal sample made by additive manufacturing. The excitation frequency is 1 Hz to neglect the eddy currents phenomena.

$$f(x) = \frac{a_0}{2} + \sum_{n=1}^{\infty} (a_n \cos(\frac{n\pi x}{p}) + b_n \sin(\frac{n\pi x}{p})) \tag{3}$$

Where a_0 represents the constant term, a_n and b_n are the Fourier coefficients for cosine and sine terms, respectively. The index n ranges from 1 to infinity. These parameters, widely recognized in the literature, are thoroughly discussed in [18–20]. In particular here, the highly efficient Fast Fourier Transform (FFT) algorithm is used to compute the Discrete Fourier Transform (DFT). When compared to conventional techniques, this method significantly lowers computational complexity, making it suitable for high-speed and real-time processing. [18,21,22]. Indeed, DFT is highly effective in breaking down time-domain signals into their individual frequency components, allowing for precise manipulation of specific elements within the frequency spectrum. In Digital Signal Processing (DSP), the DFT takes a time-domain signal as input and outputs its corresponding representation in the frequency domain. Therefore, the DFT was employed to decompose the signal into the frequency domain, deriving the coefficients a_n and b_n from the time-domain signal of B and H. Once the signal coefficients had been obtained, in order to ensure that the data were suitable for neural network input, a preliminary analysis included the standardisation of the coefficient, as recommended by [23]. In particular, StandardScaler [24], a widely used data preprocessing technique that standardizes coefficients by removing the mean and scaling them to unit variance, was applied to all coefficients. This ensures that the transformed data has a mean of 0 and a standard deviation of 1 for each coefficient. Data in this format can thus be more easily manipulated by machine learning algorithms that are sensitive to the scale of the input characteristics.

2.2. Proposed neural network architecture

ANNs have significantly advanced various scientific and engineering domains. Their application in predicting magnetic behavior [25–28] has demonstrated accurate results, reinforcing their utility in analyzing complex data and enabling the development of novel magnetic materials.

Building on these promising findings, this study proposes an ANN architecture to optimize the input-output mapping between the H and B signals, in the frequency domain. The decomposed signal, characterized by its compact representation and essential frequency components, is used to significantly optimise the efficiency of the network by mapping the frequency coefficients of B and H.

The proposed ANN model was implemented in Python using the Keras API, a high-level interface for building neural networks, and TensorFlow, a powerful open-source software library for numerical computation, as the backend. This combination provided a strong and adaptable framework for developing the personalized prediction model. The Sequential API was used to arrange the network, enabling straightforward adjustments to the neural network architecture. This flexibility facilitated the optimization of the network architecture to meet the specific requirements of the task using the described approach. The architecture was tailored to the dimensions of the input and output data, with the number of layers determined through a trial-and-error process to effectively capture the complex relationships between coefficients across various tests [29]. Model performance was evaluated using the loss function on the validation set, which quantified the error between the model's predictions and the target values during training.

The proposed ANN architecture features two hidden layers. The input layer includes two neurons, one for each input coefficient, i.e. the a_n and b_n coefficients of B. These inputs are processed by 20 neurons in the second layer and 30 neurons in the third layer. For these layers, the ReLU (Rectified Linear Unit) activation function was chosen. The ReLU function is particularly effective in mitigating the vanishing gradient problem, thereby facilitating more efficient training of deeper networks [30]. The features are then passed to a single output neuron with a sigmoid activation function, which predicts the selected coefficient. The sigmoid function is selected for its capability to map the output to a range between 0 and 1 [31], which is particularly useful for our regression task. To this end, as specified above, the data were appropriately scaled to ensure that they lie within the specified range. The architecture of the neural network is depicted in Fig. 4.

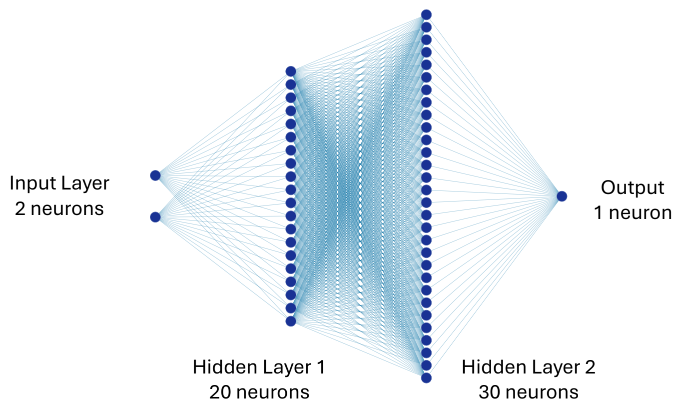

Figure 4. The architecture of the proposed ANN designed to predict the frequency coefficient of H.

The training process involved varying key hyperparameters, including the learning rate α, the decay rate of the first moment β_1, and the decay rate of the second moment β_2. The best results were achieved with the following settings: a learning rate of $\alpha = 10^{-2}$, a first-moment decay rate of $\beta_1 = 0.9$, and a second-moment decay rate of $\beta_2 = 0.999$, in line with the practical recommendations outlined in [32]. The model is compiled with the Adam optimizer, an adaptive algorithm selected for its efficiency in adjusting learning rates during training to enhance convergence, proven effective in various neural network applications [33]. We use the mean squared error (MSE) as a loss function. The MSE is appropriate for regression tasks as it penalizes larger errors more than smaller ones, leading to a model that aims to minimize significant deviations between predicted and actual values. The MSE loss function is used to measure the average of the squares of the errors, ensuring that the model focuses on minimizing these errors.

The model is trained for 300 epochs, meaning it undergoes 300 complete passes over the entire training dataset. A batch size of 100 is employed, determining the number of samples processed by the network before updating its parameters. This batch size demonstrated a good balance between memory efficiency and convergence speed for the given dataset and model architecture [34].

The model comprises a total of 2,183 parameters, occupying approximately 8.53 KB of memory. These parameters are divided into Trainable Parameters: 727 (2.84 KB), which are updated during the training process through back-propagation, Non-Trainable Parameters: 0 (0.00 KB), indicating that no fixed parameters are used in the model and Optimizer Parameters: 1,456 (5.69 KB), representing additional parameters managed by the optimizer.

Additionally, another neural network, referred to as ANN_2, was implemented for comparison. Unlike the proposed model, ANN_2 lacks the two hidden layers. For a comprehensive analysis, the Support Vector Regressor (SVR) and the Random Forest Regressor (RFR) were also considered. The SVR extends the principles of Support Vector Machines (SVM) to regression problems. It aims to identify a function that predicts the output within a specified tolerance while minimizing error [35]. Instead, the RFR is an ensemble learning algorithm that creates multiple decision trees during training and then combines their predictions to improve accuracy and prevent overfitting. For regression tasks, the output is the average prediction from all trees [36]. These two algorithms were implemented using the default parameters suggested by the Scikit-learn library [24].

In order to maximise the training data available for each iteration, we employed Leave-One-Out Cross-Validation (LOOCV). LOOCV is a special case of k-fold cross-validation where the number of folds k is equal to the number of observations in the dataset (here k=17). In addition, LOOCV ensures that the performance metrics of our model are reliable and not biased by the specific subdivision of the dataset. This approach systematically trains the model on n-1 observations and tests it on the single remaining observation, repeating this process for each observation in the dataset.

By implementing LOOCV, we obtain a comprehensive evaluation of the model's performance across all possible train-test splits. The final performance metric is calculated as the average of the metrics obtained from each iteration, providing a more stable and reliable estimate of the model's accuracy and error.

3. Results

The analysis of the dataset, consisting of 17 hysteresis loops, revealed several key insights into the impact of complexity reduction in the frequency domain. This phenomenon is exemplified in Fig. 5, which depicts the frequency domain representation of a signal segment obtained through the Fast Fourier Transform (FFT).

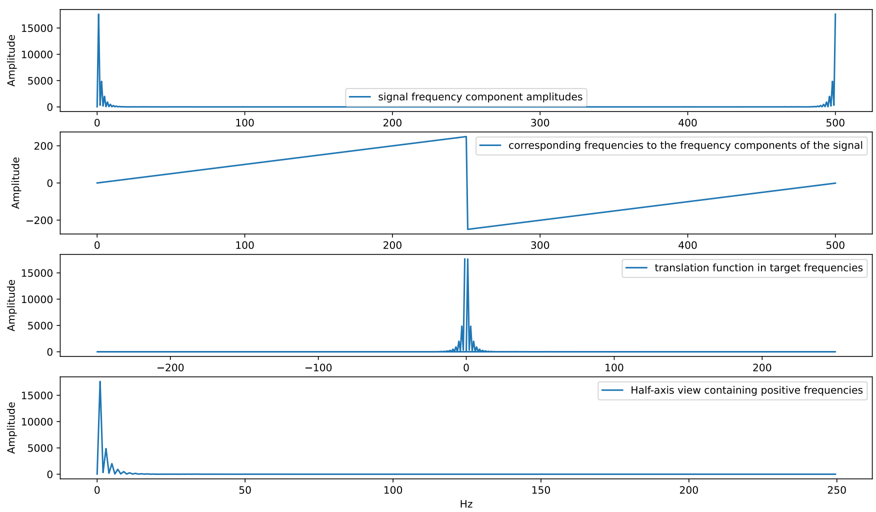

Figure 5. Frequency Spectrum Analysis of an input H as example.

The reduction proved effective in optimizing predictive tasks, and enhancing overall performance by simplifying the input-output of the neural network.

The first subplot displays the absolute values of the FFT, where each point's height represents the amplitude of a specific frequency component present in the signal. The second subplot shows the actual frequencies associated with each point in the FFT spectrum, aligning the x-axis with the signal's frequency content. The third subplot combines the information from the previous subplots, plotting the absolute FFT values (amplitudes) on the y-axis against the corresponding frequencies on the x-axis. The fourth subplot focuses on the positive half of the frequency spectrum, displaying only the non-negative frequencies and their corresponding amplitudes for a clearer view of the dominant frequency components, as the FFT result is symmetrical for real signals.

By expressing the data in the frequency domain, we obtain a significant compression of the data due to the dominance of the first harmonics. Harmonics with amplitudes below a defined threshold were discarded, retaining only frequencies with amplitudes within 98% of the maximum. This phenomenon is illustrated in Fig. 6, which provides a more concise view of the frequency spectrum and the signals obtained through the Fourier transform, focusing only on those with the highest amplitudes.

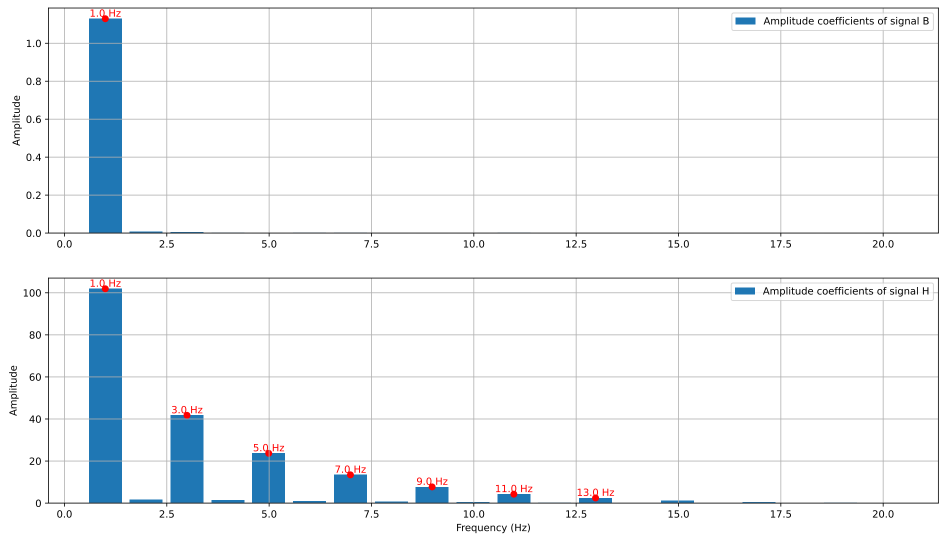

Figure 6. The plot displays the frequencies of *B* and *H*. Red circles indicate frequencies with amplitudes exceeding a threshold set at 98% below the maximum amplitude. The x-axis represents the frequency, while the y-axis corresponds to the amplitude. Only frequencies surpassing this threshold are highlighted for clarity

The plot highlights the significant coefficients to be considered. Each red dot is labeled with its corresponding frequency value in Hertz (Hz) and marks the identified peak frequencies. These peaks are determined based on their amplitudes exceeding a threshold set at up to 98% smaller than the maximum amplitude. The x-axis represents the frequency in Hz, while the y-axis denotes the amplitude of each frequency component.

Since signal *B(t)* is sinusoidal (as shown in the central graph of Fig. 3), the only component to be considered is the one related to the first harmonic; consequently, the non-zero coefficients are only those associated with the fundamental harmonic, as indicated by the upper graph in Fig. 6, the possible presence of additional harmonics, even if limited in amplitude, can be discarded as they represent noise resulting from the experimental data acquisition process. The *H(t)-signal*, on the other hand, exhibits additional harmonics, as shown in the lower graph (Fig. 6).

In particular, for the input signal *B(t)*, the fundamental harmonic at 1 Hz is sufficient for accurate signal reconstruction. In the case of the *H(t)* signal, the even harmonics have amplitudes below the threshold and can therefore be disregarded. The significant harmonics are found at frequencies of 1, 3, 5, 7, 9, 11, and 13 Hz. A reconstruction of the signal using the previously identified coefficients is shown in Fig. 7.

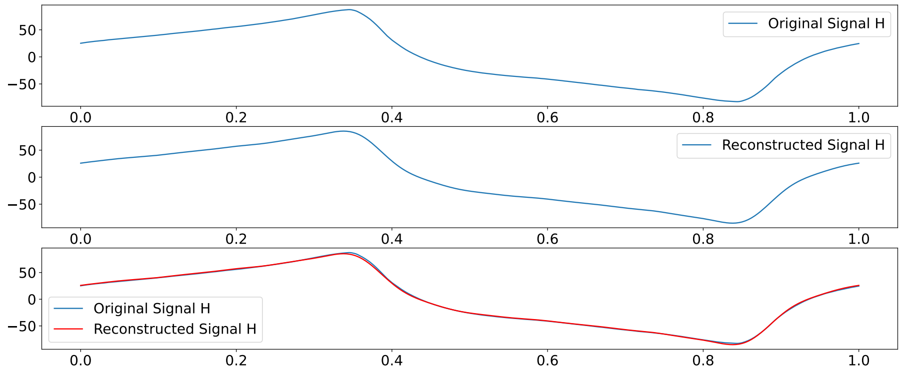

Figure 7. Comparison between the original signal 'H' and its reconstruction using harmonics at frequencies of 1, 3, 5, 7, 9, 11, and 13 Hz

An example of a complete hysteresis loop in Fig. 8.

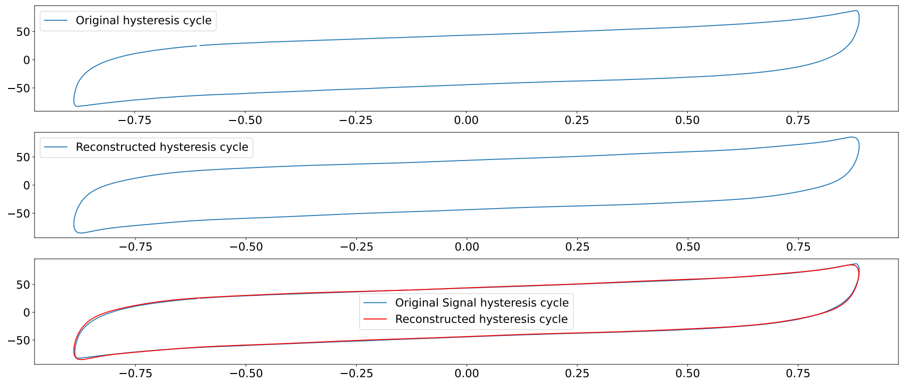

Figure 8. Comparison between the original signal hysteresis cycle and its reconstruction using the fundamental harmonics for B and at frequencies of 1, 3, 5, 7, 9, 11, and 13 Hz for H

Fig. 9 shows the reconstruction of all signals, considering only the frequencies that exceeded the previously defined threshold.

To preserve the only relevant components, the first 13 harmonics were considered, with only the odd components being retained. Consequently, each cycle of the H signal can be faithfully reconstructed using 7 a_n coefficients for the cosine component and 7 b_n coefficients for the sine component, a_0 is negligible). So each cycle of H can be faithfully reconstructed with 14 coefficients. The data compression is truly remarkable, considering values from 501 samples to 14 for H and 2 for B. This leads to a strong saving of data, concentrating the information of interest in the amplitudes of the relevant components. Therefore, the proposed model is well-suited for predicting each coefficient of H. By adopting a parallelized approach, the entire signal can be reconstructed, as illustrated in Fig. 10, which illustrates the data processing flowchart leading to the reconstruction of the original data.

To enhance the clarity of the results and concentrate on the analysis of losses, we limited our focus to the fundamental harmonic, appropriately compressing the data. Consequently, during the supervised learning process, the processing pipeline was designed to intake the coefficients a_n and b_n corresponding to the fundamental harmonic of B and accurately predict the coefficients a_n and b_n associated with the fundamental harmonic of H. This capability is crucial for estimating hysteresis losses in ferromagnetic materials, enabling the optimised design of electromagnetic devices.

The results are presented using the Mean Absolute Error (MAE), a metric commonly employed to assess the accuracy of a model's predictions. Specifically, Table 1 reports the

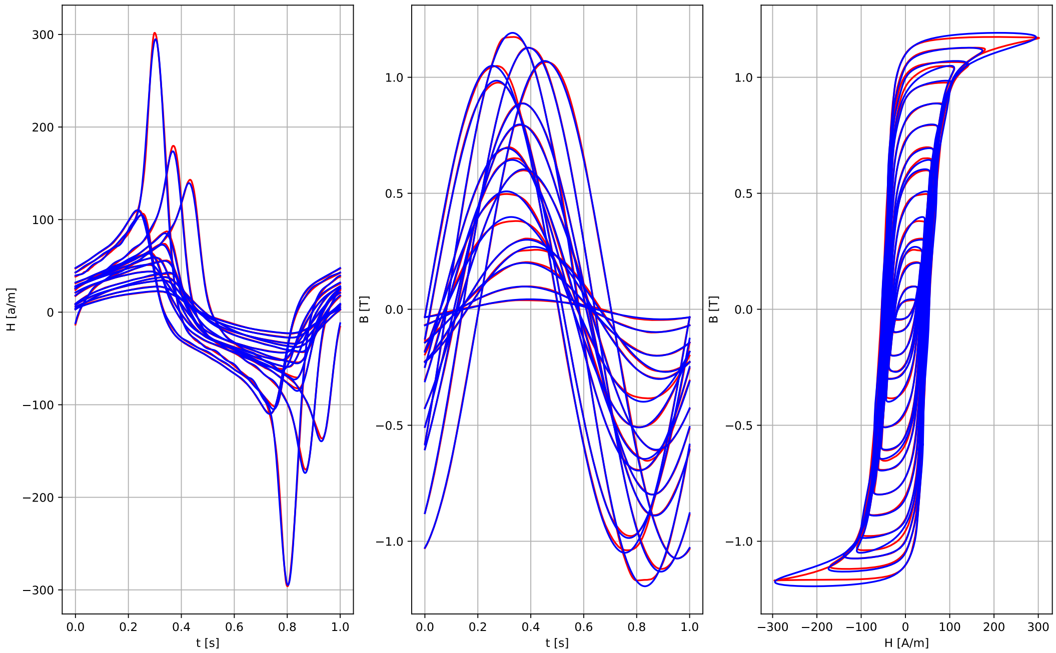

Figure 9. Experimental data (red) compared to harmonic reconstruction (blue) based on selected frequencies.

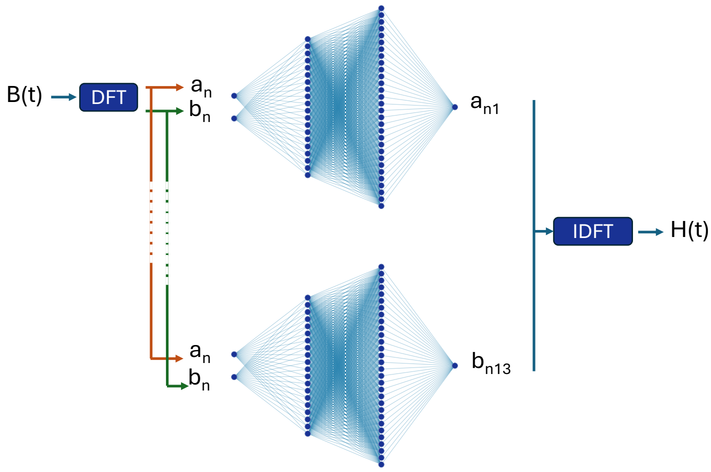

Figure 10. Flowchart illustrating the data processing pipeline, including decomposition of the signal into frequency components with the DFT, prediction of H coefficients and subsequent reconstruction of the original data with the Inverse Discrete Fourier Transform (IDFT).

MAE values evaluating the accuracy of the a_n model's predictions for the fundamental harmonic of *H(t)*, while Table 2 presents the MAE values for the b_n model's predictions on the same harmonic, with results shown for each test fold. By leveraging MAE, we quantified the predictive accuracy of the models concerning the fundamental harmonic *H(t)* within each test fold. The fundamental harmonic was selected as the focus because, in the context of sinusoidal inputs, the fundamental harmonic represents the primary component of interest when analyzing losses.

The results obtained show a low error rate in most validation folds, confirming the high accuracy of the model in estimating the amplitude of the fundamental component. Compression of the data, achieved by frequency analysis using the Fourier transform, made it possible to use a greatly simplified model, without compromising the accuracy of the results. The obtained results were compared with those of other models, specifically the previously described ANN_2, the RFR, and the SVR. The findings highlighted that the

MAE on coefficient an MAE on coefficient a_n				
Fold	**Proposed ANN**	ANN$_2$	SVR	RFR
1	**0.017**	0.116	0.072	0.220
2	**0.002**	0.130	0.056	0.162
3	**0.002**	0.105	0.089	0.103
4	**0.043**	0.086	0.056	0.022
5	**0.281**	0.556	0.502	0.374
6	**0.163**	0.161	0.089	0.058
7	**0.023**	0.014	0.069	0.028
8	**0.108**	0.030	0.015	0.249
9	**0.021**	0.176	0.050	0.039
10	**0.075**	0.041	0.076	0.075
11	**0.062**	0.461	0.183	0.208
12	**0.062**	0.006	0.054	0.067
13	**0.203**	0.172	0.076	0.121
14	**0.054**	0.237	0.067	0.231
15	**0.096**	0.223	0.066	0.008
16	**0.061**	0.103	0.060	0.009
17	**0.058**	0.038	0.032	0.097

Table 1. MAE evaluate the accuracy of a_n model's predictions on a fundamental harmonic of *H(t)* for each test fold

MAE on coefficient an MAE on coefficient b_n				
Fold	**Proposed ANN**	ANN_2	SVR	RFR
1	**0.051**	0.022	0.064	0.032
2	**0.029**	0.067	0.041	0.013
3	**0.059**	0.045	0.001	0.055
4	**0.175**	0.181	0.109	0.074
5	**0.204**	0.206	0.141	0.18
6	**0.091**	0.089	0.037	0.087
7	**0.076**	0.468	0.064	0.04
8	**0.796**	0.759	0.755	0.722
9	**0.003**	0.011	0.028	0.035
10	**0.175**	0.023	0.0	0.056
11	**0.061**	0.424	0.24	0.59
12	**0.0**	0.215	0.069	0.053
13	**0.053**	0.193	0.091	0.058
14	**0.078**	0.258	0.07	0.146
15	**0.283**	0.323	0.401	0.145
16	**0.084**	0.096	0.056	0.084
17	**0.127**	0.176	0.123	0.092

Table 2. MAE evaluate the accuracy of b_n model's predictions on a fundamental harmonic of *H(t)* for each test fold

proposed ANN achieved, on average, more accurate results than ANN_2. The latter, lacking hidden layers, failed to effectively capture the input-output nonlinearity. A similar trend was observed for the regression algorithms, with both the RFR and the SVR showing higher MAE.

These results lay the foundation for efficient loss calculation and open up new perspectives for future studies, with the opportunity to use data simulated by the neural network model instead of experimental data in subsequent investigations.

4. Discussion

This study focused on analyzing static hysteresis loops under varying excitation amplitudes, with the primary objective of examining frequency behavior to optimize a specially designed neural network architecture for predicting input-output signals. A detailed spectral analysis facilitated the optimization of the model's structure by emphasizing the first harmonic, which encapsulated the most critical information. This approach enabled significant data compression, as spectral analysis revealed that the most relevant information was concentrated within the first 13 harmonics, with a focus on the first 7 harmonics. This focus allowed for a more balanced representation of input and output data, enhancing the model's generalizability. Furthermore, the simplified model design mitigated issues related to data sparsity, leading to more reliable and robust predictions. Moreover, by disregarding higher-order harmonics, the model effectively reduced extraneous noise and improves the extraction of significant features. The results were compared with another architecture, called ANN_2, characterised by a lower number of levels, which showed a lower performance. Similarly, models such as the RFRs and SVRs were considered, which, although they obtained worse results compared to the proposed model, were able to obtain an MAE that was not too high in predicting the value of the harmonic components. These results were largely due to the change in domain, which made the information more manageable for the proposed models. Comparison with traditional models would not have been possible without this transformation, as the inherent complexity of the temporal information to be mapped would have made processing significantly more difficult. Moreover, the implementation of cross-validation maximized the utility of the training dataset, enhancing the extraction of relevant features for characterizing magnetic behavior. This strategy, designed to optimize the exploitation of available data while reducing the model's computational complexity, yielded promising results, paving the way for new applications of neural networks in magnetic material analysis.

While the current focus on first harmonic analysis enables accurate loss estimation, it imposes limitations on the full reconstruction of the hysteresis loop. Future work will involve incorporating data with variable frequencies and waveforms to enhance the neural network's generalization capabilities and provide a more comprehensive description of the underlying physical phenomena.

5. Conclusions

The present study has carried out an in-depth analysis of the temporal components of B and H, adopting an innovative approach based on the Fourier transform. This methodological choice proved to be particularly effective in the present case, characterised by a sinusoidal excitation signal, allowing for a significant compression of the data. The numerical results obtained showed a significant reduction in the dimensionality of the problem, with a consequent improvement in the computational efficiency and generability of the ANN model employed. The results obtained are encouraging and suggest that further investigation in this direction could lead to the development of more refined and versatile analysis tools. In particular, the acquisition of a larger and diversified dataset would allow the training of ANN models capable of more accurately predicting magnetic losses at different frequencies and operating conditions.

While the current focus on first harmonic analysis enables accurate loss estimation, it imposes limitations on the full reconstruction of the hysteresis loop. Future work will involve incorporating data with variable frequencies and waveforms to enhance the neural network's generalization capabilities and provide a more comprehensive description of the underlying physical phenomena.

Author Contributions: Conceptualization, M.L.G., A.S., A.F.; methodology, M.L.G., A.S., M.S., A.F.; software, M.L.G.; validation, M.L.G., A.S., M.S. F.S., S.L., G.A., P.R., V.B., A.F.; formal analysis, M.L.G., A.S.; investigation, M.L.G., A.S., M.S., A.F.; resources, F.S., G.A., A.F.; data curation, M.L.G., A.S., M.S., A.F.; writing—original draft preparation, M.L.G.; writing—review and editing, M.L.G.; visualization, M.L.G., A.S., M.S. F.S., S.L., G.A., P.R., V.B., A.F.; supervision, A.S., F.S., G.A., A.F.; project administration F.S., G.A., A.F.; funding acquisition, F.S., G.A., A.F. All authors have read and agreed to the published version of the manuscript

Acknowledgments: This work is supported under the Project No. 2022ARNLRP funded by the "European Union - Next Generation EU, Mission 4 Component 1 CUP J53D23000670006".

Conflicts of Interest: The authors declare no conflicts of interest.

Data Availability Statement: Data available on request from the authors

References

1. Rodriguez Vargas, B.; Stornelli, G.; Folgarait, P.; Ridolfi, M.R.; Miranda Pérez, A.F.; Di Schino, A. Recent Advances in Additive Manufacturing of Soft Magnetic Materials: A Review. *Materials* **2023**, *16*, 5610.
2. Naseer, M.U.; Kallaste, A.; Asad, B.; Vaimann, T.; Rass~olkin, A. A review on additive manufacturing possibilities for electrical machines. *Energies* **2021**, *14*, 1940.
3. Stornelli, G.; Faba, A.; Di Schino, A.; Folgarait, P.; Ridolfi, M.R.; Cardelli, E.; Montanari, R. Properties of additively manufactured electric steel powder cores with increased Si content. *Materials* **2021**, *14*, 1489.
4. Di Schino, A.; Montanari, R.; Sgambetterra, M.; Stornelli, G.; Varone, A.; Zucca, G. Heat treatment effect on microstructure evolution of two Si steels manufactured by laser powder bed fusion. *Journal of Materials Research and Technology* **2023**, *26*, 8406–8424.
5. Tiismus, H.; Kallaste, A.; Belahcen, A.; Rassolkin, A.; Vaimann, T.; Shams Ghahfarokhi, P. Additive Manufacturing and Performance of E-Type Transformer Core. *Energies* **2021**, *14*, 3278.
6. Tiismus, H.; Kallaste, A.; Naseer, M.U.; Vaimann, T.; Rassolkin, A. Design and Performance of Laser Additively Manufactured Core Induction Motor. *IEEE Access* **2022**, *10*, 50137–52.
7. Gargalis, L.; Madonna, V.; Giangrande, P.; Rocca, R.; Hardy, M.; Ashcroft, I.; Galea, M.; Hague, R. Additive Manufacturing and Testing of a Soft Magnetic Rotor for a Switched Reluctance Motor. *IEEE Access* **2020**, *8*, 206982–91.
8. Goodall, A.D.; Nishanth, N.; Severson, E.L.; Todd, I. Loss Performance of an Additively Manufactured Axial Flux Machine Stator with an Eddy-Current Limiting Structure. *Materials Today Communications* **2023**, *35*, 105978.
9. Preisach, F. Über die magnetische Nachwirkung. *Z. Phys.* **1935**, *94*, 277–302.
10. Jiles, D.C.; Atherton, D. Ferromagnetic hysteresis. *IEEE Trans. Magn.* **1983**, *19*, 2183–2185.
11. Bergqvist, A. Magnetic Vector Hysteresis Model with Dry Friction-like Pinning. *Physica B* **1997**, *233*, 342–347.
12. Kumar, A.; Arockiarajan, A. Evolution of nonlinear magneto-elastic constitutive laws in ferromagnetic materials: A comprehensive review. *Journal of Magnetism and Magnetic Materials* **2022**, *546*, 16882.
13. Faba, A.; Riganti Fulginei, F.; Quondam Antonio, S.; Stornelli, G.; Di Schino, A.; Cardelli, E. Hysteresis modelling in additively manufactured FeSi magnetic components for electrical machines and drives. *IEEE Transaction on Industrial Electronics* **2024**, *71*, 2188–2197.
14. Quondam Antonio, S.; Riganti Fulginei, F.; Laudani, A.; Faba, A.; Cardelli, E. An effective neural network approach to reproduce magnetic hysteresis in electrical steel under arbitrary excitation waveforms. *Journal of Magnetism and Magnetic Materials* **2021**, *528*, 167735.
15. Quondam-Antonio, S.; Riganti-Fulginei, F.; Laudani, A.; Lozito, G.M.; Scorretti, R. Deep neural networks for the efficient simulation of macro-scale hysteresis processes with generic excitation waveforms. *Engineering Applications of Artificial Intelligence* **2023**, *121*, 105940.
16. *EN IEC 60404-6 - Magnetic Materials - part 6: Methods of measurement of the magnetic properties of magnetically soft metallic and powder materials at frequencies in the range 20 Hz to 100 kHz by the use of ring specimens.*, 2018.
17. Wahab, M.F.; Gritti, F.; O'Haver, T.C. Discrete Fourier transform techniques for noise reduction and digital enhancement of analytical signals. *TrAC Trends in Analytical Chemistry* **2021**, *143*, 116354.
18. Developers, N. *NumPy: Discrete Fourier Transform (`fft`).* NumPy Project, https://numpy.org. Accessed: 17/04/2024.
19. Brunton, S.L.; Kutz, J.N. *Data-Driven Science and Engineering: Machine Learning, Dynamical Systems, and Control*; Cambridge University Press, 2019.
20. Sneddon, I.N. *Fourier transforms*; Courier Corporation, 1995.
21. Brigham, E. The Fast Fourier Transform and its Applications, 1988.
22. Sundararajan, D. *The discrete Fourier transform: theory, algorithms and applications*; World Scientific, 2001.

23. Anysz, H.; Zbiciak, A.; Ibadov, N. The influence of input data standardization method on prediction accuracy of artificial neural networks. *Procedia Engineering* **2016**, *153*, 66–70.
24. scikit-learn developers. *StandardScaler — scikit-learn 1.4.0 documentation*, 2024. Accessed: 2024-11-22.
25. Quondam Antonio, S.; Fulginei, F.R.; Lozito, G.M.; Faba, A.; Salvini, A.; Bonaiuto, V.; Sargeni, F. Computing frequency-dependent hysteresis loops and dynamic energy losses in soft magnetic alloys via artificial neural networks. *Mathematics* **2022**, *10*, 2346.
26. Farrokh, M.; Dizaji, F.S.; Dizaji, M.S. Hysteresis identification using extended preisach neural network. *Neural Processing Letters* **2022**, pp. 1–25.
27. Quondam Antonio, S.; Bonaiuto, V.; Sargeni, F.; Salvini, A. Neural network modeling of arbitrary hysteresis processes: Application to GO ferromagnetic steel. *Magnetochemistry* **2022**, *8*, 18.
28. Licciardi, S.; Ala, G.; Francomano, E.; Viola, F.; Giudice, M.L.; Salvini, A.; Sargeni, F.; Bertolini, V.; Di Schino, A.; Faba, A. Neural Network Architectures and Magnetic Hysteresis: Overview and Comparisons. *Mathematics* **2024**, *12*, 1–23.
29. Chollet, F. The Sequential model - Keras: Python deep learning library, 2023.
30. Hara, K.; Saito, D.; Shouno, H. Analysis of function of rectified linear unit used in deep learning. In Proceedings of the 2015 international joint conference on neural networks (IJCNN). IEEE, 2015, pp. 1–8.
31. Menon, A.; Mehrotra, K.; Mohan, C.K.; Ranka, S. Characterization of a class of sigmoid functions with applications to neural networks. *Neural networks* **1996**, *9*, 819–835.
32. Bengio, Y. Practical recommendations for gradient-based training of deep architectures. In *Neural networks: Tricks of the trade: Second edition*; Springer, 2012; pp. 437–478.
33. Kingma, D.P. Adam: A method for stochastic optimization. *arXiv preprint arXiv:1412.6980* **2014**.
34. Hwang, J.S.; Lee, S.S.; Gil, J.W.; Lee, C.K. Determination of Optimal Batch Size of Deep Learning Models with Time Series Data. *Sustainability* **2024**, *16*, 5936.
35. Awad, M.; Khanna, R.; Awad, M.; Khanna, R. Support vector regression. *Efficient learning machines: Theories, concepts, and applications for engineers and system designers* **2015**, pp. 67–80.
36. scikit-learn developers. *RandomForestRegressor — scikit-learn 1.4.0 documentation*, 2024. Accessed: 2024-11-22.